ChemCatChem

Research Article
doi.org/10.1002/cctc.202200932

Chemistry Europe
European Chemical Societies Publishing

www.chemcatchem.org

On the Role of Interfacial Water Dynamics for Electrochemical Stability of RuO_2 and IrO_2

Iman Evazzade[+],[a] Alexandra Zagalskaya[+],[a, b] and Vitaly Alexandrov*[a, c]

Based on the coincident onsets of oxygen evolution reaction (OER) and metal dissolution for many metal-oxide catalysts it was suggested that OER triggers dissolution. It is believed that both processes share common intermediates, yet exact mechanistic details remain largely unknown. For example, there is still no clear understanding as to why rutile IrO_2 exhibits such an exquisite stability among water-splitting electrocatalysts. Here, we employ density functional theory calculations to analyze interactions between water and the (110) surface of rutile RuO_2 and IrO_2 as a response to oxygen evolution involving lattice oxygen species. We observe that these oxides display qualitatively different interfacial behavior that should have important implications for their electrochemical stability. Specifically, it is found that IrO_2(110) becomes further stabilized under OER conditions due to the tendency to form highly stable low oxidation state Ir(III) species. In contrast, Ru species at RuO_2(110) are prone to facile reoxidation by solution water. This should facilitate the formation of high Ru oxidation state intermediates (>IV) accelerating surface restructuring and metal dissolution.

Introduction

Water electrolysis is one of the most promising ways to store renewable energy.[1–5] The four-electron oxygen evolution reaction (OER) at the anode is characterized by more sluggish kinetics than the two-electron hydrogen evolution reaction (HER) at the cathode. To split water electrochemically, cost-effective electrocatalysts for both half-cell reactions are urgently needed. Despite the high cost, noble metal-based catalysts remain the materials of choice for electrocatalytic water splitting owing to their favorable combination of activity-stability properties. The exceptional activity of RuO_2 and superior stability of IrO_2 in the rutile phase made their mixed oxides viable electrocatalysts for OER in acidic solutions.[6,7] By getting the best of both worlds allows one to reduce the loading of scarce and expensive Ir metal in acidic proton exchange membrane water electrolyzers (PEMWE). To enable the most economical solution numerous prior studies have investigated the properties of $Ir_xRu_{1-x}O_2$ series as a function of their composition, morphology and catalyst pretreatment.

Despite years of research, our mechanistic understanding of the interplay between electrocatalytic activity and corrosion remains surprisingly poor even for the most studied Ir-based oxides. This is because the primary emphasis of research community has been on understanding OER activity, while atomic-scale investigations of OER-driven corrosion have started to emerge only recently.[8–16]

It is believed that dissolution of metal-oxide electrocatalysts is triggered by OER based on the observations of the coincident onsets of OER and dissolution; however, mechanistic details remain under intense discussion. Among various factors of lattice instability, the so-called lattice oxygen mechanism (LOM) is considered[3,12,14,16,17] and was directly correlated with dissolution of Ir in iridium oxides.[10,11] In a recent study, a quantitative assessment of the lattice oxygen involvement and the degree of Ir dissolution was performed for rutile IrO_2.[11] It was shown that despite its exceptional electrochemical stability rutile IrO_2 does feature O_2 evolution from the oxide lattice. Specifically, it was found that OER triggers an exchange of oxygen atoms in the topmost 2.5 nm of the IrO_2 lattice facilitating surface restructuring and degradation. It was estimated that approximately 1×10^{11} lattice oxygen atoms per second are directly involved in the OER mechanism under the applied electrochemical conditions. In addition, it was assessed that one Ir atom dissolves per approximately 33 exchanged lattice oxygen atoms from rutile IrO_2. In contrast, Ir hydrous oxide was found to be highly unstable due to substantial lattice oxygen participation in OER causing a much faster dissolution of Ir. An important role of lattice oxygen activation in inducing lattice instability was also demonstrated for $SrIrO_3$ electrocatalyst.[18] Overall, lattice oxygen involvement in OER was observed in a wide range of metal-oxide electrocatalysts, but its actual role in materials stability is not well understood.[16]

[a] Dr. I. Evazzade,[+] Dr. A. Zagalskaya,[+] Prof. Dr. V. Alexandrov
Department of Chemical and Biomolecular Engineering,
University of Nebraska-Lincoln,
Lincoln, Nebraska 68588, United States
E-mail: valexandrov2@unl.edu
[b] Dr. A. Zagalskaya[+]
Quantum Simulations Group, Materials Science Division,
Lawrence Livermore National Laboratory,
7000 East Ave., Livermore, California 94550, United States
[c] Prof. Dr. V. Alexandrov
Nebraska Center for Materials and Nanoscience,
University of Nebraska-Lincoln, Lincoln,
Nebraska 68588, United States
E-mail: valexandrov2@unl.edu
[+] These authors contributed equally.

A related question concerning LOM and its role in catalyst degradation is what happens with the newly formed defect site after O_2 is released from the oxide lattice. It was discussed that the evolved lattice oxygen species can be replenished either through diffusion of oxygen atoms from the bulk to the surface or via dissociation of water molecules producing oxygenated species that refill the vacancy sites (likely a much more facile process). The generation of such oxygen vacancies via LOM and their subsequent refilling are directly related to surface restructuring and degradation. Therefore, it was proposed that surface oxygen exchange kinetics could potentially serve as a stability descriptor for OER electrocatalysts.[11]

We also want to point out that experimental investigations of dynamic interfacial properties of OER electrocatalysts are plagued with many challenges affecting interpretation of experimental observations. Even determination of such a basic property as the oxidation state of Ir at Ir-based electrode surfaces during OER remains highly debated. Different studies pointed to the presence of Ir in oxidation states equal to, lower and higher than +4. Here, we refer to a recent viewpoint[19] discussing some technical issues such as catalyst delamination and the formation of O_2 bubbles that can lead to experimental artifacts and erroneous data interpretations on the example of IrO_2-based materials. In this regard, modeling of idealized electrode/electrolyte interfaces offers an obvious advantage.

In this study, we employ DFT based simulations to investigate surface reoxidation process under OER conditions. Given previous studies suggesting the involvement of lattice oxygen in OER and its detrimental effect on lattice stability for a number of oxides, we aim to analyze how the electrode/electrolyte interface responds to LOM. With this goal, we focus on two OER materials exhibiting low (RuO_2) and high (IrO_2) stabilities during OER as our model systems.

Results and Discussion

To compare the propensity of RuO_2 and IrO_2 surfaces toward reoxidation as a result of the OER, we carry out AIMD simulations with explicit water environment at the interface. Although it is established that LOM becomes much more favorable at the defect sites of these rutile oxides,[12,14] we consider here the ideal flat (110) surface of RuO_2 and IrO_2 as a simplified model. We then create a number of oxygen vacancies that would be formed during OER via LOM and analyze a surface response to this perturbation in the presence of surrounding water molecules.

We find that the IrO_2(110) surface forms the structures characterized by decreased Ir–Ir distances relative to the regular rutile lattice, as shown in Figure 1a. This occurs due to the preference of the surface to restructure in such a way that the Ir species form new Ir–O bonds with surface O rather than being reoxidized back to the original rutile structure. By using the Bader charge analysis we identify these species as Ir(III). Such Ir(III) were previously hypothesized to form during electrochemical cycling of IrO_2 electrocatalysts.[20] Our finding also agrees with recent experimental observations using operando

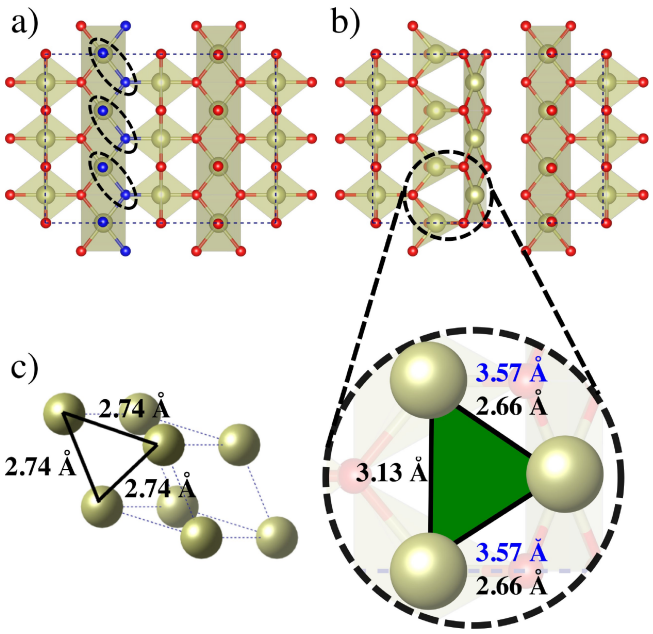

Figure 1. Top view of the IrO_2(110) surface before (a) and after (b) removal of three O_2 species (depicted in blue) as a result of OER via LOM. A close-up picture for structure (b) shows the outcome of structural optimization after three O_2 were removed. The Ir–Ir interatomic distances are listed for the initial rutile (in blue) and final distorted (in black) structures. It is seen that the formed Ir triangles in the distorted structure are characterized by Ir–Ir distances significantly reduced relative to those in the original rutile structure and being now comparable to those in metallic Ir (see structure c).

X-ray absorption spectroscopy[15] indicating decreased Ir–Ir distances at the IrO_2 surface at OER potentials above 1.5 V vs. reversible hydrogen electrode (RHE). In contrast, we observe that the RuO_2(110) surface rapidly reoxidizes back by dissociating water molecules from solution (see Figure 1b). This behavior is consistent with a more reactive nature of Ru species. These results suggest that the dynamics of interfacial water is drastically different at the IrO_2 and RuO_2 surfaces.

We next analyze the implication of such electrolyte/electrode interactions for surface stability. Since we observe that the oxygen vacancies at the RuO_2(110) surface are rapidly refilled by dissociated water, here we only model dissolution of Ir from restructured IrO_2(110). Previously, we have already simulated dissolution of transition metals (Ru and Ir) from the perfect MO_2(110) (M = Ru or Ir) surface into aqueous solution using accelerated free-energy AIMD calculations.[13,29] In particular, it was found that the activation barrier of 1.7 eV is needed for the first bond-breaking event, leading to Ir species forming bonds with the nearest oxygens on the surface. To get a fully dissolved Ir complex in solution, the activation barrier of 0.55 eV is required, resulting in the total dissolution barrier of 2.25 eV. Figure 2 shows the free-energy profile for Ir(III) dissolution obtained from our blue-moon AIMD simulations in this work. It can be seen that the energy barrier for Ir(III) dissolution is significantly increased relative to the one for Ir(IV). This is because the first transition from Ir(III) to Ir(IV) requires a high barrier of almost 3 eV. The activation barrier for the second transition from Ir(IV) to Ir(V) is found to be smaller (~1.2 eV)

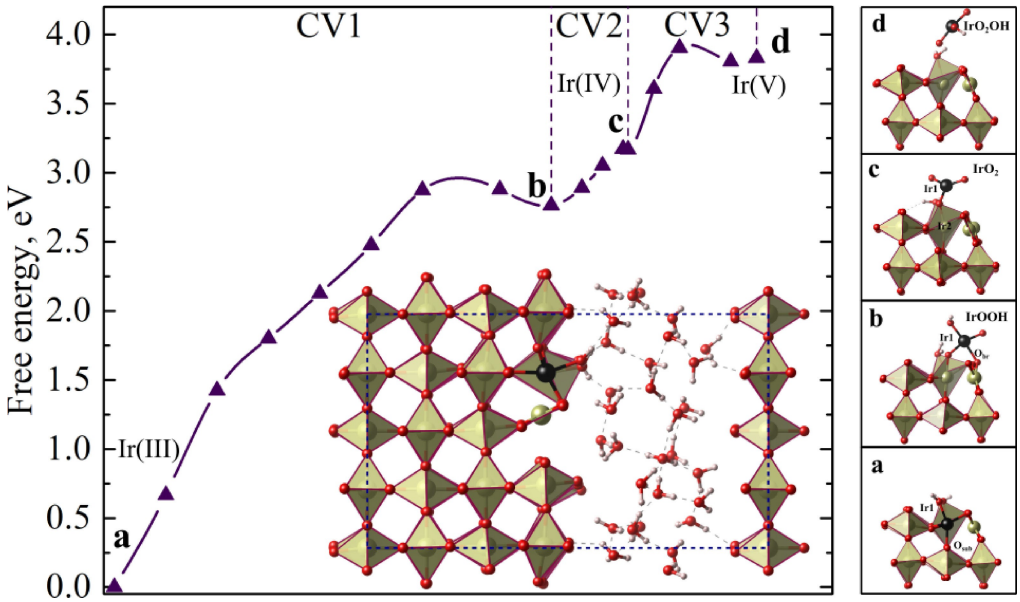

Figure 2. Free-energy profile ($\triangle G$) of Ir dissolution from the reduced IrO_2(110) surface. The corresponding metastable structures along the dissolution pathway are shown in the inset: a) initial reduced structure (after O_2 was removed), b) IrOOH intermediate formed by dissolving Ir, c) IrO_2 formed after breaking the bond with the surface oxygen atom, d) final state IrO_2OH in solution. The change in oxidation state is presented along the dissolution profile. The right panel demonstrates the choice of CVs: the initial CV1 corresponds to the distance between Ir1 and subsurface oxygen O_{sub}; CV2 is chosen as the distance between Ir1 and O_{br}, the final CV3, d(Ir1-Ir2), dissolves the Ir1 atom into solution completely.

being comparable to our previous value obtained for Ir dissolution from the perfect IrO_2(110) surface.[13] This result indicates a low propensity for reoxidation of oxygen-deficient IrO_2(110) compared to RuO_2(110). This should therefore lead to surface passivation impeding Ir dissolution.

To complement these AIMD insights into the electrode/electrolyte interactions, we carry out an additional thermodynamic analysis based on computational stability diagrams. Figure 3 shows the computed surface stability diagrams for the regular (a) and distorted (b) structures of IrO_2(110). The distorted structure corresponds to the one obtained after the removal of surface oxygen molecules followed by the optimization of atomic positions. The final optimized structure turned out to be equivalent to the one obtained using AIMD equilibration. These static optimization calculations can serve as an additional validation of our AIMD results.

The stability diagrams shown in Figure 3 reveal that the potentials of surface oxidation are significantly increased for the distorted IrO_2(110) surface relative to the regular case. Specifically, we can find that the potential at which the surface becomes completely oxygen covered (red line) shifts from 1.94 V_{SHE} for the regular structure (Figure 3a) to 2.18 V_{SHE} for the distorted structure (Figure 3b). A similar shift can be observed for the partially oxidized surfaces such as for the green line corresponding to 50% OH coverage of the cus sites with all the bridge sites being oxidized. In this case the potential shift from 1.35 V_{SHE} for the ideal structure to 1.50 V_{SHE} for the distorted structure. Such higher oxidation potentials for the distorted

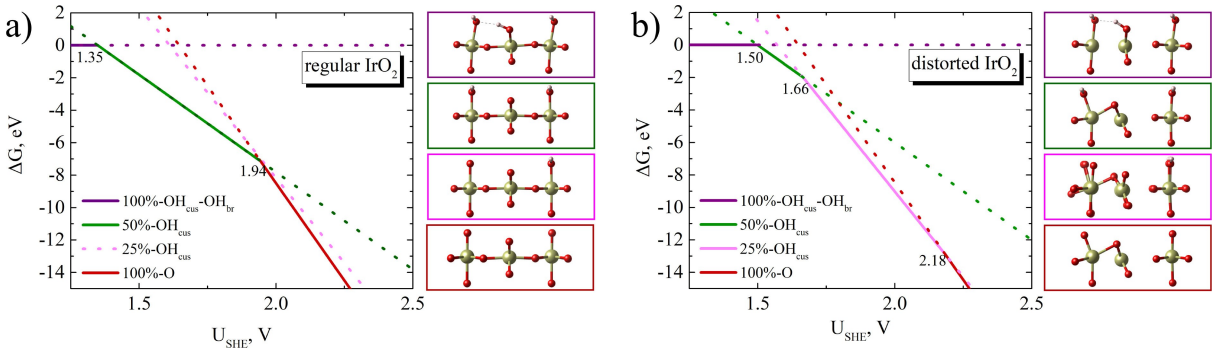

Figure 3. Surface phase diagrams of a) regular IrO_2(110), b) distorted IrO_2(110). 100%-OH coverage (purple line) corresponds to fully OH-terminated surface, where both OH_{cus} and OH_{bri} are protonated. 50%-OH coverage (green line) corresponds to the protonated OH_{cus} sites, while O_{bri} are oxidized. In case of 25%-OH coverage (magenta), half of OH_{cus} sites is protonated, half of O_{cus} and all O_{bri} are oxidized. 100%-O (red line) corresponds to fully oxidized surface (O_{cus} and all O_{bri}).

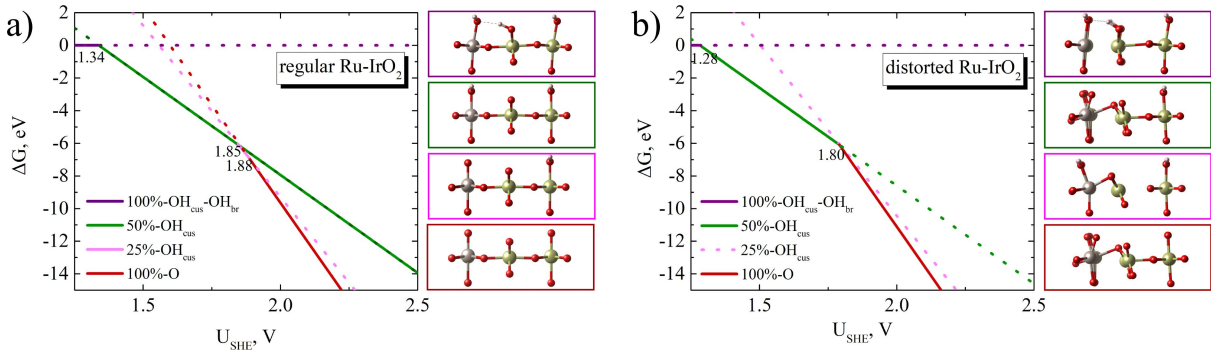

Figure 4. Surface stability diagrams of a) regular $Ru_{16.7}Ir_{83.3}O_2$(110), b) distorted $Ru_{16.7}Ir_{83.3}O_2$(110). The mixed structures correspond to two Ru species substituting Ir atoms at the neighboring cus sites.

IrO_2(110) surface indicate its greater stability under OER conditions. This is also consistent with a higher barrier of Ir dissolution obtained from AIMD for this structure (see Figure 2) as additional energy is required to first oxidize and then dissolve Ir.

Recently, mixed rutile-type $Ir_xRu_{1-x}O_2$ oxides have been investigated as the OER anodes due to their favorable combination of activity and stability characteristics.[7] The greater stability is attributed to the presence of IrO_2 phase, while the higher OER activity is owing to RuO_2. What is interesting, however, is the experimental observation of a non-linear relationship between composition of mixed oxide nanoparticles and metal dissolution. Specifically, it was demonstrated that the addition of only 20 at.% Ir to RuO_2 resulted in a 10-fold decrease in Ru dissolution with minimal reduction of the OER activity.[7] As a result, the systems with 20 at.% Ir and 80 at.% Ir in the RuO_2 matrix are characterized by comparable levels of Ru dissolution. This occurs, however, at the expense of Ir stability in the $Ir_xRu_{1-x}O_2$ matrix relative to pure IrO_2. We refer the reader to the original study for more details.

Here, we attempt to rationalize these observations of non-linear relationships between electrochemical stability of $Ir_xRu_{1-x}O_2$ and its composition given our present results on interfacial water dynamics. First of all, we plot the computed surface diagrams for the mixed-oxide system considering the regular and distorted models (Figure 4). It can be observed that the potentials for complete surface oxidation expectedly become lower in the mixed case relative to the pure IrO_2 surfaces for both regular (1.88 vs. 1.94 V) and distorted (1.80 vs. 2.18 V) models. This appears to be consistent with experimental data showing decreased stability of Ru-doped IrO_2 relative to the undoped oxide. Combining all these computational and experimental results, we come up with a mechanism that can explain a non-linear relationship between stability and $Ir_xRu_{1-x}O_2$ composition. Figure 5 schematically summarizes the proposed mechanism. First, we note that Ru species are known to leach out from the surface faster than Ir under OER conditions. This will create metal vacancies on the surface which presence was shown to promote OER via LOM.[12] However, our results discussed above reveal that such an Ir-enriched surface tends to form the structures characterized by decreased Ir–Ir distances,

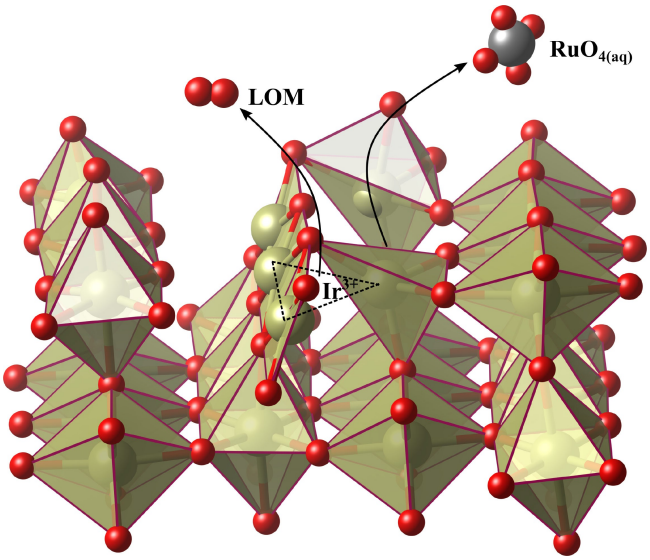

Figure 5. The schematic representation of the proposed mechanism of dissolution and surface restructuring for $Ir_xRu_{1-x}O_2$.

i.e., containing Ir(III) species. As we discussed earlier, this should impede Ir dissolution. Such protection layer should at the same time limit Ru leaching out from subsurface layers thereby leading to a self-passivating effect.

Conclusion

The obtained computational results highlight an important role of interfacial water dynamics in surface reoxidation during OER affecting the overall electrochemical stability of $Ir_xRu_{1-x}O_2$ electrocatalysts. Specifically, we find that a more facile reoxidation kinetics of the RuO_2(110) surface facilitates the formation of high Ru oxidation state intermediates (>IV) thus promoting Ru dissolution. However, this is not the case for IrO_2 that is more prone to form low oxidation state Ir(III) intermediates on the surface due to the lower oxophillicity of Ir. These intermediates are characterized by much higher dissolu-

tion barriers that should result in Ir enrichment on the surface with a self-protecting effect.

Based on our modeling results, we also propose a mechanistic model describing stability of the mixed $Ir_xRu_{1-x}O_2$ catalysts including an experimentally detected non-linear relationship between the catalyst's stability and composition. The mechanism suggests that the added Ru species being more prone to dissolution thus leaving metal vacancies behind will promote LOM. Healing of the surface oxygen vacancies formed as a result of LOM is expected to be much slower around the Ir sites. This will lead to the formation of stable surface structures involving Ir(III) species thereby minimizing further dissolution of Ru species from subsurface layers. We believe that our findings on the role of water/electrode interactions in electrochemical stability of $Ir_xRu_{1-x}O_2$ should be generalizable to other OER electrocatalysts.

Computational Approach

Electronic-structure calculations in this work were performed within the density functional theory (DFT) framework as implemented in the Vienna Ab initio Simulation Package (VASP).[21,22] The revised Perdew-Burke-Ernzerhof (revPBE) exchange-correlation functional[23,24] and projector augmented wave (PAW) potentials (Ir, Ru_pv, O, H) were employed.[25,26] A cut-off energy of 400 eV was used in all calculations. The D3 approach according to the Grimme formalism[27,28] was employed to account for non-local van der Waals interactions. Periodic four-layer slab models of the MO_2(110) rutile surface (M = Ir, Ru) were constructed using a 2×3 surface supercell. $Ir_xRu_{1-x}O_2$ models were created by doping the IrO_2(110) surface. Distorted structures were created by removal of one to three O_{cus}-O_{lat} pairs as demonstrated in Figure 1. A vacuum gap of about 10 Å was used to minimize periodic image interactions. For slab optimizations the bottom layer of each slab was fixed to the bulk positions, while the top three layers were allowed to relax. The convergence criteria for total energies and atomic forces were set to 10^{-6} eV and 0.02 eV/Å, respectively, during structural optimization.

To investigate the electrochemical stability of the regular and defective oxides, we constructed the surface phase diagrams using equations (Eq. 1–3). We considered pH = 0, therefore a free energy correction related to pH is not included.

$$^* + nH_2O \leftrightarrow nO_{cus}{}^* + 2n(H^+ + e^-),$$
$$\Delta G_{100\%O^*} = G_{nO^*} + 2nG_{H^+} - G^* - nG_{H_2O} - 2nU_{SHE} \quad (1)$$

$$^* + nH_2O \leftrightarrow nOH_{cus}{}^* + n(H^+ + e^-),$$
$$\Delta G_{25\%/50\%OH^*} = G_{nOH^*} + nG_{H^+} - G^* - nG_{H_2O} - nU_{SHE} \quad (2)$$

$$O_{br}{}^* + nH_2O \leftrightarrow OH_{br}OH_{cus}{}^*,$$
$$\Delta G_{100\%OH^*} = G_{OH_{br}OH_{cus}*} - nG_{H_2O} \quad (3)$$

Ab initio molecular dynamics (AIMD) simulations were undertaken to examine the evolution of the surface structures as a response to the OER process. Similar to the methodology[13,14,29] applied to examine the regular oxidized surfaces, we studied the reduced (distorted) structures. The slab/water systems were equilibrated using explicit water environment for at least 20 ps. To keep the water density around 1 g/cm^3, we fill the vacuum region with 27 explicit molecules. In our dissolution modeling employing the blue-moon approach, we used the distance between the topmost Ir and subsurface O atoms as an initial collective variable (CV1) to push Ir into solution with a velocity of 0.5 Å/ps. The further CVs we discuss in detail in Figure 2. Each state in the free energy profile presented in Figure 2 was equilibrated for 2 ps, following 3 ps averaging of forces over the time frame. A time step of 1.0 fs and the H mass of 3 amu were set in AIMD simulations. The Nose-Hoover thermostat was chosen to keep the temperature around 300 K in our simulations.

Acknowledgements

We acknowledge funding support from the National Science Foundation (NSF) through the NSF CAREER award (Grant No. CBET-1941204). This research used resources of the National Energy Research Scientific Computing Center, a DOE Office of Science User Facility supported by the Office of Science of the U.S. Department of Energy under Contract No. DE-AC02-05CH11231, as well as the Holland Computing Center at the University of Nebraska-Lincoln.

Conflict of Interest

The authors have no conflicts of interest to declare.

Data Availability Statement

The data that support the findings of this study are available from the corresponding author upon reasonable request.

Keywords: Corrosion · Electrocatalysis · Noble metal oxides · Oxygen evolution reaction · Water dynamics

[1] H. Over, *Chem. Rev.* **2012**, *112*, 3356, pMID: 22423981.
[2] Y. Jiao, Y. Zheng, M. Jaroniec, S. Z. Qiao, *Chem. Soc. Rev.* **2015**, *44*, 2060.
[3] E. Fabbri, T. J. Schmidt, *ACS Catal.* **2018**, *8*, 9765.
[4] A. M. Oliveira, R. R. Beswick, Y. Yan, *Curr. Opin. Chem. Eng.* **2021**, *33*, 100701.
[5] Z. Pu, T. Liu, G. Zhang, H. Ranganathan, Z. Chen, S. Sun, *ChemSusChem* **2021**, *14*, 4636.
[6] H. Over, *ACS Catal.* **2021**, *11*, 8848.
[7] D. Escalera-López, S. Czioska, J. Geppert, A. Boubnov, P. Röse, E. Saraçi, U. Krewer, J.-D. Grunwaldt, S. Cherevko, *ACS Catal.* **2021**, *11*, 9300.
[8] E. Fabbri, M. Nachtegaal, T. Binninger, X. Cheng, B.-J. Kim, J. Durst, F. Bozza, T. Graule, R. Schäublin, L. Wiles, M. Pertoso, N. Danilovic, K. E. Ayers, T. J. Schmidt, *Nat. Mater.* **2017**, *16*, 1476.
[9] O. Kasian, J.-P. Grote, S. Geiger, S. Cherevko, K. J. J. Mayrhofer, *Angew. Chem. Int. Ed.* **2018**, *57*, 2488.
[10] O. Kasian, S. Geiger, T. Li, J.-P. Grote, K. Schweinar, S. Zhang, C. Scheu, D. Raabe, S. Cherevko, B. Gault, K. J. J. Mayrhofer, *Energy Environ. Sci.* **2019**, *12*, 3548.

[11] K. Schweinar, B. Gault, I. Mouton, O. Kasian, *J. Phys. Chem. Lett.* **2020**, *11*, 5008, pMID: 32496784.
[12] A. Zagalskaya, V. Alexandrov, *ACS Catal.* **2020**, *10*, 3650.
[13] A. Zagalskaya, V. Alexandrov, *J. Phys. Chem. Lett.* **2020**, *11*, 2695, pMID: 32188249.
[14] A. Zagalskaya, I. Evazzade, V. Alexandrov, *ACS Energy Lett.* **2021**, *6*, 1124.
[15] S. Czioska, A. Boubnov, D. Escalera-López, J. Geppert, A. Zagalskaya, P. Röse, E. Saraçi, V. Alexandrov, U. Krewer, S. Cherevko, J.-D. Grunwaldt, *ACS Catal.* **2021**, *11*, 10043.
[16] K. S. Exner, *ChemCatChem* **2021**, *13*, 4066.
[17] C. E. Beall, E. Fabbri, T. J. Schmidt, *ACS Catal.* **2021**, *11*, 3094.
[18] G. Wan, J. W. Freeland, J. Kloppenburg, G. Petretto, J. N. Nelson, D.-Y. Kuo, C.-J. Sun, J. Wen, J. T. Diulus, G. S. Herman, Y. Dong, R. Kou, J. Sun, S. Chen, K. M. Shen, D. G. Schlom, G.-M. Rignanese, G. Hautier, D. D. Fong, Z. Feng, H. Zhou, J. Suntivich, *Sci. Adv.* **2021**, *7*, eabc7323.
[19] N. Diklić, A. H. Clark, J. Herranz, J. S. Diercks, D. Aegerter, M. Nachtegaal, A. Beard, T. J. Schmidt, *ACS Energy Lett.* **2022**, *7*, 1735.
[20] D. F. Abbott, D. Lebedev, K. Waltar, M. Povia, M. Nachtegaal, E. Fabbri, C. Coperet, T. J. Schmidt, *Chem. Mater.* **2016**, *28*, 6591.
[21] G. Kresse, J. Furthmüller, *Phys. Rev. B* **1996**, *54*, 11169.
[22] G. Kresse, J. Furthmller, *Comput. Mater. Sci.* **1996**, *6*, 15.
[23] J. P. Perdew, K. Burke, M. Ernzerhof, *Phys. Rev. Lett.* **1996**, *77*, 3865.
[24] Y. Zhang, W. Yang, *Phys. Rev. Lett.* **1998**, *80*, 890.
[25] P. E. Blöchl, *Phys. Rev. B* **1994**, *50*, 17953.
[26] G. Kresse, D. Joubert, *Phys. Rev. B* **1999**, *59*, 1758.
[27] S. Grimme, J. Antony, S. Ehrlich, H. Krieg, *J. Chem. Phys.* **2010**, *132*, 154104.
[28] S. Grimme, S. Ehrlich, L. Goerigk, *J. Comput. Chem.* **2011**, *32*, 1456.
[29] K. Klyukin, A. Zagalskaya, V. Alexandrov, *J. Phys. Chem. C* **2019**, *123*, 22151.

Manuscript received: July 25, 2022
Revised manuscript received: September 17, 2022
Accepted manuscript online: September 26, 2022
Version of record online: ■■, ■■■

RESEARCH ARTICLE

The graphical TOC illustrates the competition between oxygen evolution reaction involving lattice oxygen species and surface reoxidation. This equilibrium depends on the nature of the electrode and operating conditions with implications for electrode stability.

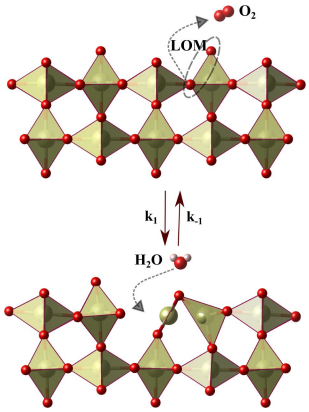

*Dr. I. Evazzade, Dr. A. Zagalskaya, Prof. Dr. V. Alexandrov**